8-28-2024

A NOVEL PERFUSED CONTUSION SPINAL CORD INJURY MODEL TO ASSESS RAPID MECHANICAL PROPERTIES CHANGES AFTER BLOOD SPINAL CORD BARRIER BREAKDOWN

Laura De Marchi
Rowan University

A NOVEL PERFUSED CONTUSION SPINAL CORD INJURY MODEL TO ASSESS RAPID MECHANICAL PROPERTIES CHANGES AFTER BLOOD SPINAL CORD BARRIER BREAKDOWN

by

Laura De Marchi

A Thesis

Submitted to the
Department of Biomedical Engineering
Henry M. Rowan College of Engineering
Rowan-Virtua School of Translational Biomedical Engineering and Sciences
In partial fulfillment of the requirement
For the degree of
Master of Science in Biomedical Engineering
at
Rowan University
June 26th, 2024

Thesis Chair: Peter A. Galie, Ph.D., Associate Professor and Translational Research Chair, Department of Biomedical Engineering

Committee Members:
Patrick Hwang, Ph.D., Assistant Professor, Department of Biomedical Engineering
Sophia Orbach, Ph.D., Assistant Professor, Department of Biomedical Engineering

Dedication

A mamma e papá,

per avermi mostrato cosa significhi essere forti e altruisti,

e alla mia puzzikona,

per avermi insegnato come vivere con coraggio e determinazione.

To the arts we want to keep alive and the sciences we want to understand.

To the crafts we try to master and the ones we learn to value.

Acknowledgments

I would like to express my sincere gratitude to Dr. Peter A. Galie, my thesis supervisor, for his invaluable guidance and unwavering support throughout my experience at Rowan University. His expertise and encouragement have been instrumental in shaping this work.

I am also grateful for the help and encouragement from my fellow graduate students Louis Paone and Evan Hutt. Their contributions are greatly appreciated.

This thesis would not have been possible without the support and encouragement of all those mentioned above, as well as countless others who have played a role, however small, in its completion.

Abstract

Laura De Marchi
A NOVEL PERFUSED CONTUSION SPINAL CORD INJURY MODEL TO ASSESS RAPID MECHANICAL PROPERTIES CHANGES AFTER BLOOD-SPINAL CORD BARRIER BREAKDOWN
2023-2024
Peter A. Galie, Ph.D.
Master of Science in Biomedical Engineering

Blood-spinal cord barrier (BSCB) disruption exacerbates the tissue damage caused by spinal cord injury (SCI), but the mechanisms and dynamics of how the barrier breakdown affects the mechanical properties of the tissue remain unclear. The perfused bovine ex vivo indentation injury model described here represents a new platform to investigate the short-term effects of altered blood flow and vascular permeability following traumatic spinal cord injury. Our results indicate that injured cords exhibit changes to bulk perfusion, as evidenced by laser speckle contrast imaging, in addition to decreased barrier function shortly after injury. Indentation tests that simultaneously simulate a crush injury and provide force-indentation data reveal that tissue softening initiates as early as 30 minutes when perfused with whole blood. Perfusing with resuspended RBC (rRBC) instead of whole blood mitigates the decreased stiffness, highlighting the importance of white blood cells and plasma proteins in mediating the extracellular matrix mechanical response after SCI. Immunohistochemical staining indicates increased levels of extravasated Evans blue, ED-1, and vimentin in injured sections, suggesting mechanisms underlying the rapid response in mechanical properties following injury. This research provides novel insights into the immediate mechanical and vascular changes following spinal cord injury.

Table of Contents

Table of Contents (Continued)

List of Figures

Chapter 1

Introduction

Spinal cord injury (SCI) is defined as damage to the spinal cord that often causes loss of strength and sensation below the sites of the injury and can be caused by either a traumatic or non-traumatic event. Despite the promising results of recent studies, a lack of characterization between the biological consequences of SCI and the mechanical response of the nervous tissue to a traumatic event hinders the effectiveness of possible therapeutical approaches to improve patients' lifestyles. The research presented here introduces a new perfused ex vivo model for traumatic spinal cord injury that functions as a novel platform to study the relationship between the blood spinal cord barrier (BSCB) breakdown and the mechanical changes of the spinal cord tissue after traumatic injury.

Epidemiology

Traumatic spinal cord injury has affected an average of 305,000 people since 2015, and 18,000 new injuries are estimated to occur each year in the United States alone. Male victims comprise of 79% of total victims, and Non-Hispanic White people are the most affected at 55.5%. The most traumatic events causing spinal cord injury are vehicular accidents (37.5%), falls (31.7%), and violence (15.4%), followed by sports accidents, medical procedures, and other traumatic events (Fig. 1)[1]. The neurological level and extent of injury, which depends on the severity and location of the traumatic injury, includes permanent motor dysfunctions, which can vary from incomplete tetraplegia (47.7%) to incomplete paraplegia (20%), complete paraplegia (19.7%) and complete tetraplegia (12.3%), as well as chronic cognitive and behavioral effects [1]. Despite recent advances in rehabilitation and treatment, patients with traumatic spinal

cord injury have a significantly shorter lifespan than their age-matched control groups [3].

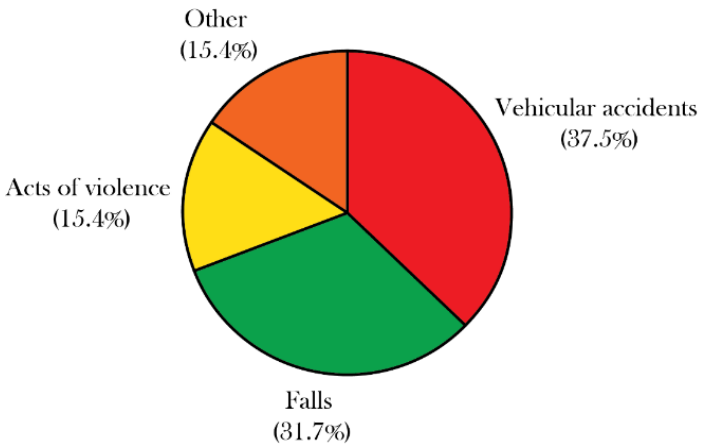

Figure 1. Causes of traumatic Spinal Cord Injury [1]

Spinal Cord Anatomy

The spinal cord, the main path of communication between the brain and the peripheral nerves, is a continuation of the brain stem that elongates from the medulla oblongata to the sacral region of the spine through the vertebral foramen [4] (Fig. 2). The epidural space, between the spine and the outermost layer of the spinal cord, is filled with adipose tissue and contains an intricate network of blood vessels[5]. The dura mater and the arachnoid mater, the outer and middle meninges respectively, are the two protective coating layers of the spinal cord and are connected to the pia mater, the innermost layer, through denticulate ligaments[5]. The subarachnoid space, between the arachnoid and pia mater encloses another layer of vasculature that delivers most of the blood supply to the spinal cord (Fig. 2). Three major arteries, one anterior and two posteriors, run along the sides of the spinal cord and split into smaller radical arteries

which are responsible for penetrating the tissue and providing most of the nutrients to the glial cells in the white and grey matter[6]. The anterior spinal cord artery (ASA) is responsible for two thirds of the total vasculature supply, while the two posterior arteries provide blood for the posterior third[6]. Because the arteries run alongside the whole cord, they need additional arterial supply through radiculomedullary arteries, branches of the radicular artery, to maintain the blood supply consistent at the different anatomical levels. Blood supply to the ASA is replenished at the cervical-thoracic, mid-thoracic, and thoracic-lumbar level creating three areas where the flow is both ascending and descending, referred to as retrograde flow [2, 6] (Fig. 3). The tissue of the spinal cord is divided into two main layers, white and grey matter, which present different mechanical and physiological properties. The white matter is the outermost layer, and it is mostly comprised of myelinated sensory and motor axons, which transport information from the brain to the peripheral nerves. The grey matter, conversely, consists mostly of neuronal cell bodies, glial cells (astrocytes and oligodendrocytes), neuropil (dendrites and unmyelinated axons), and capillaries, which create a control center for all the information to be processed and controlled. Mechanically, the spinal cord has shown a heterogeneous nature through tensile, shear, compression [7, 8], and magnetic resonance elastography [9, 10]. Although atomic force microscopy (AFM) testing has been done to support bulk measurements on a smaller scale, published studies show contradictory information regarding differences in the mechanical properties of the white and grey matter[11, 12]. Whereas some studies found that grey matter is stiffer than white matter in all anatomical planes[13], others show a possible lack of significance between the two types of tissue[11]. Previous AFM and tensiometry studies from our lab indicated that the grey

matter exhibits a higher elastic moduli and relaxation factor compared to the white matter for all anatomical levels (cervical, lumbar, and sacral)[14].

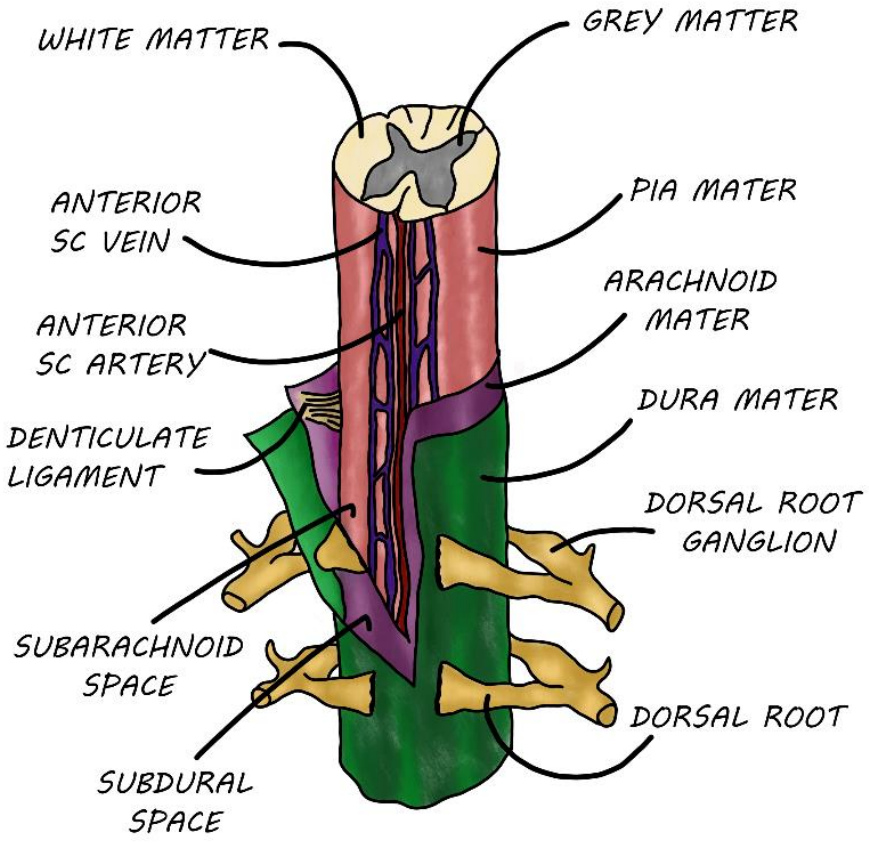

Figure 2. Spinal Cord Diagram

Pathophysiology of Traumatic Spinal Cord Injury

Traumatic spinal cord injury can be divided physiologically by primary or secondary injury or temporally in acute (<48 hours), subacute (48 hours – 14 days), intermediate (14 days to 6 months) and chronic (> 6 months) phases (Fig. 3).

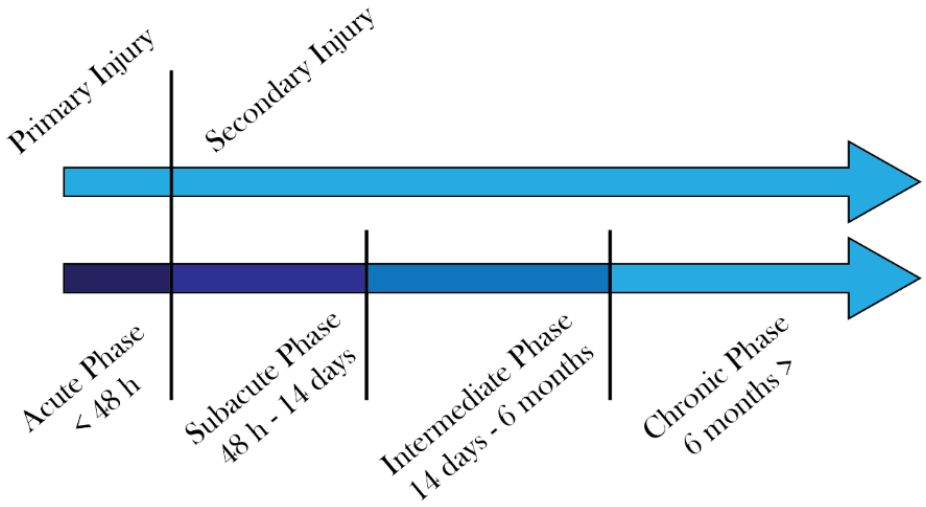

Figure 3. Physiological and temporal timelines of spinal cord injury

An initial traumatic event causes a fragment of the spine to disrupt and dislocate inside the foramen distressing the spinal cord[15-17]. The compressive, distractive, or lacerating impact of the tissue causes disruption to the vasculature surrounding the spinal cord as well as to the cell membranes and neurons in the injury area [18-21]. The rupture of the barrier causes hemorrhage that leads to the influx of inflammatory cells and cytokines in the parenchymal tissue as well as ischemic injury to the lower parts of the matrix that are not reached by the blood supply[19, 22]. Within minutes of the traumatic event, microglia activate, change their morphology, and start releasing of pro-inflammatory cytokines such as interleukin-1β (IL-1β) and tumor necrosis factor (TNF) [23-25]. In the following minutes, astrocytes activate and start expressing elevated levels of glial fibrillary acidic protein (GFAP) as well as releasing more pro-inflammatory cytokines [23]. During the acute phase of injury, the recruited inflammatory cells, in addition to blood leaking into the tissue due to the BSCB breakdown, causes swelling in the immediate injury area that results in damage to the surrounding tissue.

During the subacute phase, levels of damage-associated molecular patterns (DAMPs) increase, including proteins, purine metabolites, and DNA components [20-22]. Alongside this, activated microglia and infiltrating inflammatory cells migrate towards the injury site, altering the biochemical environment of the extracellular matrix. Furthermore, the byproducts of phagocytosis and elevated levels of glutamate released by dying neurons are inadequately cleared from the extracellular matrix by surviving astrocytes, leading to further spread and aggravation of the injury [26].

The overwhelming cell death, the continuous inflammatory response, and the altered biochemical environment facilitate the formation of cystic cavities and a glial scar following the acute and sub-acute phases of injury. Cystic cavities are usually found at the interface between the white and grey matter and are characterized by increased extracellular fluid, thin bands of connective tissue and macrophages [27]. On the borders of the cystic cavity, reactive astrocytes create a mechanical barrier by releasing ECM proteins that have shown to have inhibitory characteristics to axonal growth, such as chondroitin sulfate proteoglycans (CSPGs) and NG2 proteoglycans [28, 29]. To replace the loss of the tissue, fibroblasts migrate towards the center of the region and deposit collagen and fibrous connective tissue [27]. Historically, it was believed that the glial scar had biochemical and mechanical inhibitory effects, prevented axon regeneration, and impeded full recovery from spinal cord injury. However, studies have shown that the complete ablation of the glial scar does not increase axons elongation through the injury area while preventing astrocytes activation and glial scar formation through GFAP knock-out models exacerbated the injury [30, 31]. These results suggested that the glial scar has both inhibitory and ameliorating effects in tissue regeneration and that more

characterization is needed to understand the dichotomy of glial scarring and its effects on the injury response.

A unique characteristic of glial scar formation is the effects of biochemical changes on the continuously altered mechanical properties after spinal cord injury. Recent studies observe correlations between altered ECM composition present in the spinal cord tissue throughout the subacute and intermediate phase and the mechanical properties of the tissue. The results of these studies reveal that increased values of vimentin, laminin, and collagen IV correlate with a higher percentage decrease in elastic moduli of the injured section compared to controls [32]. Additionally, another group's results show that as the injury progresses through the acute, intermediate, and chronic phases, the elastic moduli value increases and surpasses the original levels, suggesting that, as the extracellular matrix reaches a plateau state, gliosis renders the injury area stiffer than the surrounding healthy matrix [33, 34].

Recent advancements in tissue engineering show that therapeutic biomaterials have better regenerative results when the mechanical properties of the implanted scaffold or hydrogel match the properties of the host tissue [35-37]. Glial cells have high sensitivity to mismatches in mechanical properties of recent therapeutic approaches[38, 39], which may explain the benefit of matching the mechanical properties of implantable scaffolds and injectable hydrogel to surrounding tissue. Recent studies support the hypothesis that matching the mechanical properties of the spinal cord increases axon elongation effects both when the treatments exhibit homogeneous properties [40], and heterogeneous properties matching the mechanical differences of the grey and white

matter [14]. These results demonstrate the importance of improved characterization of the mechanical properties in the aftermath of spinal cord injury.

Current Studies

Ex Vivo Models

Ex vivo models provide a platform to assess tissue properties in nearly real-time due to the increased access and augmented control over the environment. Specifically, organotypic slice culture (OSC) models have been previously used to study the biochemical post-traumatic events of spinal cord injury [41-43] as well as to test cell response to possible drug treatments [44, 45]. Multiple studies have shown that OSC conserves both parenchymal and vascular tissue complexity of the slices while guaranteeing significant viability up to 14 days after insult [46-50]. Although the controlled environment makes current ex vivo models a useful platform, their inability to perfuse blood flow through the tissue vasculature is a major limitation given the importance of BSCB breakdown in the injury process. Changes to both bulk blood flow and microvascular barrier integrity cannot be modeled in OSC platform without the addition of whole blood flow.

In Vivo Models

Currently, in vivo models are preferred to study the biochemical impact of spinal cord injury on the mechanism in the subacute and intermediate phases. The different methods of monitoring and assessing the barrier, in addition to motor function tests available for mice and rats, make in vivo models extremely valuable to study longer term consequences of SCI and possible therapeutic treatments.

Additionally, in vivo studies have been developed to assess changes in spinal cord blood flow in the aftermath of SCI. Laser speckle contrast imaging (LSCI) relies on refracted scattered light to detect changes in superficial vasculature. Due to the system's ability to continuously monitor the superficial vasculature and detect small changes in perfusion velocity, LSCI has recently been used to monitor changes in perfusion levels after traumatic brain injuries and tSCI [51, 52], however the small penetration depth and sensitivity to sample motion limits LSCI applicability in in vivo studies. Recently, studies have demonstrated substantial advances in the capability of ultrasound to visualize blood flow in the injured spinal cord [53],[54]. These studies indicate that the local area of spinal cord injury undergoes a substantial decrease in whole blood perfusion. Ultrasounds imaging relies on high-frequency sound waves to create an image and can provide information on both superficial and deep tissue vasculature [55, 56]. Although ultrasounds alone are uncapable to measure changes in tissue properties, a novel ultrasounds elastography application can investigate the tissue stiffness and elasticity non-invasively and in real time. Ultrasounds elastography has been used to measure changes in mechanical properties in a variety of tissues [57-60], but few applications have been shown in spinal cord injury[61, 62].

Despite monitoring the spinal cord vasculature and blood flow has improved our understanding of the effects of BSCB breakdown after injury, the economic drawbacks of in vivo studies as well as the limited control on environmental conditions are major limitations that interfere in making spinal cord regeneration a more accessible area of study.

Aim

As more studies show the importance of matching the mechanical properties of the spinal cord in novel therapeutical approaches [14, 40], characterizing the time-dependent mechanisms underlying the loss of mechanical properties following tSCI and their basis in biochemical changes is crucial. To overcome the perfusion limitations of ex vivo models and the temporal limitations of in vivo models, which focus mostly on long-term effects of an injury, this study aims to clarify further mechanisms of rapid mechanical degradation using a perfused ex vivo model. The early stages of injury are important because they trigger key responses that either influence the healing response or further the damage to the tissue. By focusing on this immediate phase, the study aims to understand detailed mechanisms that could lead to better treatments for reducing initial damage and improving recovery. This thesis introduces a bovine perfused ex vivo indentation model that allows for mechanical and biochemical characterization of the extracellular matrix in the first hour after a spinal cord crush injury. Furthermore, the results shown test our hypothesis that the immediate biochemical changes in the ECM environment cause a decrease in elastic moduli within minutes of injury and support previous findings holding the inflammatory response a key factor in ECM mechanical properties loss [32, 33].

Chapter 2

Methods

aCSF Solution Preparation

Dissecting artificial cerebral spinal fluid (aCSF) was prepared using a previous model to maintain spinal cord tissue viability [14, 33, 34]. The solution includes 191 mM sucrose, 0.75 mM K-gluconate, 1.25 mM KH_2PO_4, 26 mM $NaHCO_3$, 4 mM $MgSO_4$, 1 mM $CaCl_2$, 20 mM glucose, 2 mM kynurenic acid, 1 mM (+)-sodium L-ascorbate, 5 mM ethyl pyruvate, 3 mM myo-inositol, and 2 mM NaOH. All the reagents were purchased from VWR, and solutions were prepared the day prior to spinal cord isolation and kept at 4˚C.

Spinal Cord and Blood Preparation

Bovine spinal cords were extracted at Bringhurst Meats (Berlin, NJ) and immediately submerged into ice-cold aCSF within minutes of death. Bovine blood was collected in a quart-sized container at Bringhurst Meats (Berlin, NJ) with 10 mL of a 10 mM sodium citrate solution and maintained on ice until the time of perfusion to prevent coagulation. At the time of experiment, the sections of the cord that were damaged during the extraction procedure were discarded and the remaining ones were divided into 10 cm sections. For experiments involving perfusion of resuspended red blood cells, a 50 mL conical tube of whole blood was centrifugated at 1000 x g for 10 minutes, the plasma and buffy coat were removed, and the volume was replaced with 1x PBS to maintain the original hematocrit.

Crush Injury Model and Indentation Mechanical Characterization

All the experiments were performed at room temperature within 6 hours of extraction, as studies have shown that submerging the spinal cord tissue in aCSF preserves its biological properties during that time span [14, 33, 34]. The dura mater was carefully removed from an approximately 10-cm long spinal cord section to access the vasculature surrounding the pia mater. A spherical indenter with a 5 mm radius was attached to the top plate of a Shimadzu mechanical tester, and a compressive force was applied to the anterior side of the spinal cord section 5 cm away from its edges at a deformation rate of 6 mm/s for a 6 mm indentation to simultaneously exert a crush injury and collect force-deformation data (Fig. 4 A,B). The different testing conditions included non-perfused groups and sections perfused with either whole blood or reconstituted red blood cells (rRBC). Non-perfused groups were resubmerged in the aCSF bath, while perfused groups were cannulated through the ASA with a 25-gauge needle immediately after the contusion injury and connected to an Arduino-controlled battery-powered peristaltic pump to mimic blood flow. For tensiometry testing, the extendable arm of a Kibron probe was placed above the spinal cord section and measurements were taken repetitively within the first 60 minutes after a <1 mm indentation. In contrast, indentation with the mechanical tester was performed for a depth of 6 mm after perfusing for 15, 30, and 60 minutes. Temperature studies were performed by perfusing the spinal cord either at room temperature or in a warm room at 37˚C. Different sections were used for each individual timepoint. The elastic moduli values at the time of injury and at varying time points were calculated applying Hertz model to the impact force measurements collected

by the mechanical tester. Least squares fitting was used to calculate the elastic modulus using contact theory (Fig. 5).

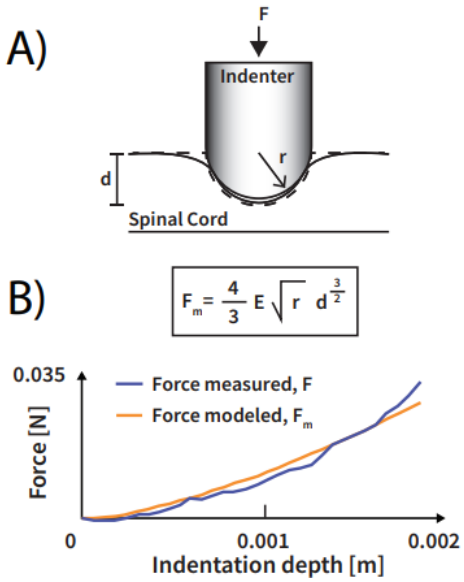

Figure 4. Mechanical indentation schematic. (A) Contusion injury model. (B) Force-indentation data for Hertz elastic moduli approximation.

Laser Speckle Contrast Imaging

A portable laser speckle contrast imaging (LSCI) device (RFLSI-ZW, RWD Life Science) with a near-infrared laser diode at 785 nm was mounted on the bench countertop with an extendable arm and used to monitor blood flow for up to 60 minutes after crush injury. The imager containing the laser diode and the camera was positioned perpendicular to the area of injury about 16 cm above the spinal cord section and the focus was adjusted to image an area of about 3.82x2.86 cm^2. Images were taken at a frame rate of 15 fps with an exposure time of 20 ms for 5 seconds and analyzed through the device software to collect blood perfusion units (BPU) averages and standard deviations values for the region of interests selected. The quantification of the LSCI

images was performed by normalizing the BPU mean over the injury region of interest to the BPU mean over the control region of interest. At least six measurements for both conditions (injured and non-injured) were obtained over the period of an hour and subjected to linear regression analysis.

Bovine Spinal Cord Immunohistochemistry

Bovine spinal cord sections were washed in PBS and fixed in 4% paraformaldehyde for 30 minutes. After fixation, the sections were embedded in OCT compound and cryopreserved at −80 °C. Each section was cut into 20 μm slices with a cryostat and mounted on microscope slides. The slides were washed with phosphate buffered saline with Triton X-100 (PBST) and blocked with 1% normal donkey serum for 1h at room temperature. The slides were incubated for 24 hours in a solution consisting of 0.1% normal donkey serum and anti-CD68 primary antibodies (VWR) diluted at a ratio of 1:100 or anti-vimentin primary antibodies diluted at a ratio of 1:100. The slides were washed 3x in PBS and secondary antibodies were added at a ratio of 1:100 and incubated at room temperature for 2 hours. After thoroughly washing the slides with PBS, they were mounted in anti-fading mounting media containing DAPI stain and conserved at 4°C. For vimentin staining, the slides were not permeabilized to preserve extracellular vimentin on cell membranes, and only washed with PBS, blocked with 1% normal donkey serum for 1h at room temperature. Primary antibodies were diluted 1:100 and incubated in the fridge overnight, while secondary antibodies were diluted at 1:100 and incubated at room temperature for 2h. The slides were mounted in anti-fading mounting medium containing DAPI stain and conserved at 4°C.

Confocal Microscopy

Immunohistological slides of the bovine spinal cord sections were imaged on a Nikon A1 laser scanning confocal microscope. Image processing and quantification was done in ImageJ and Excel. The Evans blue was quantified by measuring the ratio of intensity within the lumen and in the extravascular space (Fig. 5A-B). At least three measurements were made in distinct blood vessels to calculate an average and standard deviation. ED-1 staining was quantified by measuring the variance over a selected area that included a blood vessel to determine the extent of activation in the surrounding tissue (Fig. 6C). Finally, vimentin was quantified by measuring the ratio of intensity in the lining of vasculature compared to that in the extravascular space. These normalizations were necessary to quantify the histological results.

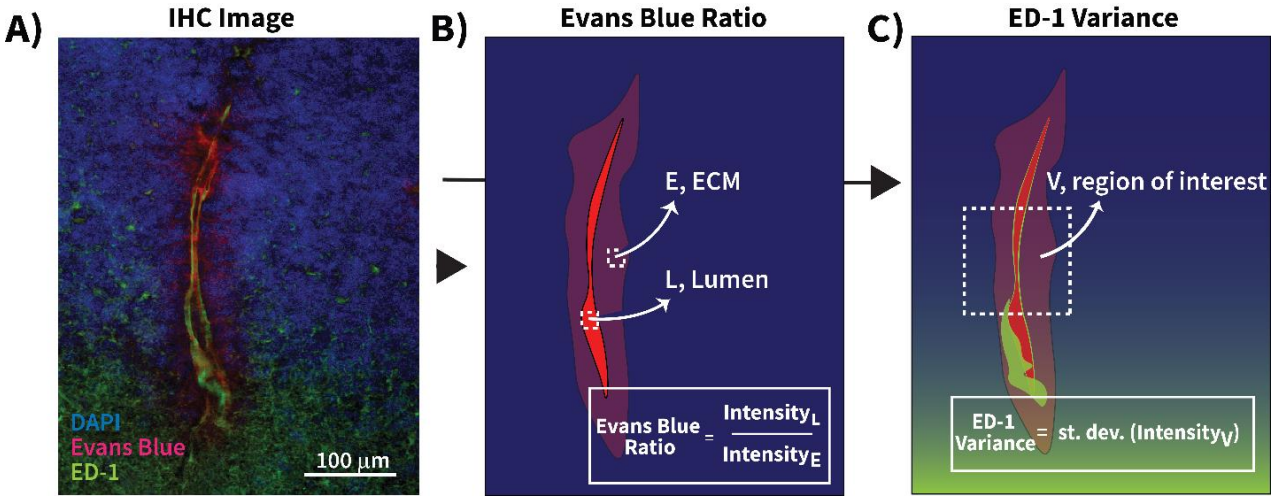

Figure 5. Schematic showing the quantification method for an example IHC image (A) for Evans Blue Ratio (B) and ED-1 variance (C).

COMSOL Multiphysics Model

The spinal cord injury model was developed in COMSOL Multiphysics using a linear elastic constitutive equation to model the indentation of the ex vivo model at 6 mm/s for 1 s. The spinal cord was designed in SolidWorks to match the average measurements of the bovine spinal sections used (5x1.9x10 cm) and the difference in elastic moduli between the white and grey matter taken from a previous study [33]. The indenter was simulated in COMSOL with a diameter of 5 mm. The contact between the two surfaces was modeled through the penalty method by adjusting the penalty factor at 0.75 and Von Mises Stress was observed at a coronal cross-section at the centerline of the indenter.

Statistics

The mechanical testing experiments were performed in triplicate on sections derived from 16 distinct ex vivo spinal cords. The laser speckle contrast imaging was performed on two separate sections of the same cord (one non-injured control and one injured section) over a one-hour time frame with $n > 6$ measurements for each sample. Immunohistochemical staining was performed on slides from the same section of the spinal cord, but each sample was from a different animal ($n = 5$). Two-sample t tests, one-way ANOVA, and post-hoc Tukey's HSD tests were used to calculate the statistical significance of our results. Statistical significance between different perfusion conditions at the same time points were calculated using two samples t-tests, assuming normal conditions and unequal variances. All p-values lower than 0.05, 0.01, 0.001 were reported as *, **, *** respectively.

Chapter 3

Results

Ex Vivo Model Validation

The primary advantage of the ex vivo model described here is the ability to perfuse whole blood through the vasculature while maintaining the ability to characterize spinal cord tissue properties. Figure 6A shows the workflow of the ex vivo experiments. Spinal cords were isolated directly into artificial cerebrospinal fluid (aCSF), which has previously been used to preserve ex vivo tissue for mechanical testing, as determined by staining for myelin at several time points [14]. Pial vasculature perfusion was verified by circulation of 1 wt% Evans Blue-Bovine Serum Albumin solution (Fig. 6B), and 2MDa-FITC dextran in saline was used to ensure successful perfusion through the parenchymal vascular bed. Coronal sections of the white and grey matter show the latter displays a higher density of vasculature following perfusion with the FITC-dextran, and that the ex vivo approach is capable of perfusing both penetrating arteries but also the microvasculature of the grey matter (Fig. 6C-D).

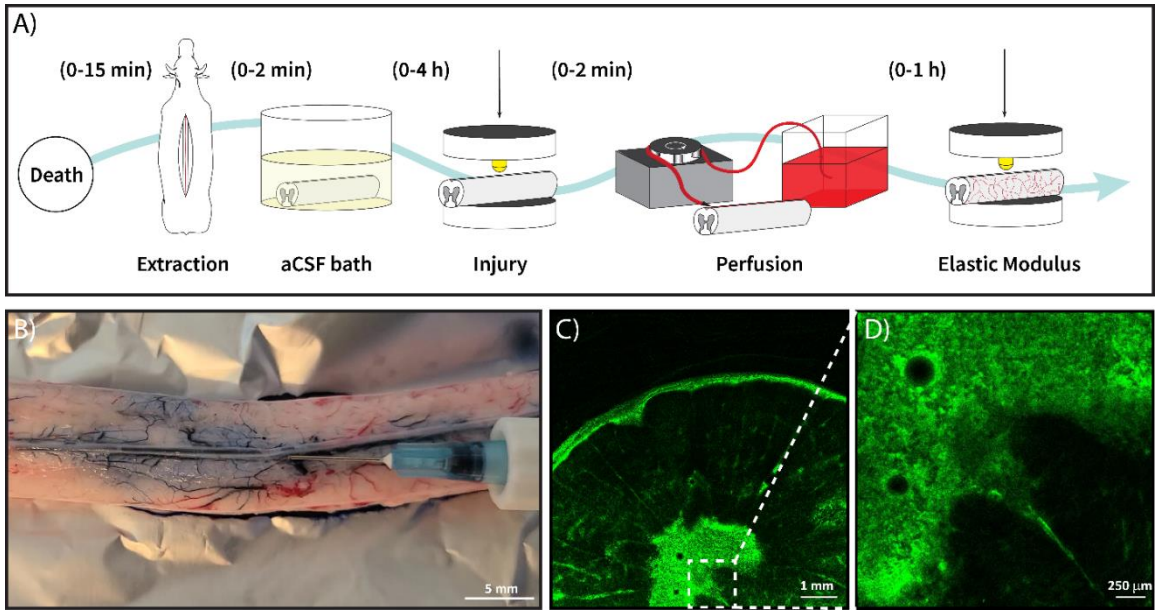

Figure 6. Ex vivo perfused model schematic and validation. (A) Schematic of compression model. (B) Perfusion of Evans Blue and (C) Coronal sections following perfusion with 2MDa – FITC Dextran.

Changes in Pial Vasculature Perfusion

Having demonstrated the ability to perfuse the ex vivo model, laser speckle contrast imaging was used to evaluate the effects of injury on blood flow in the pial vasculature. Figure 7A-B shows the flux heatmap images comparing the changes in superficial perfusion between an uninjured control section (Fig. 7A, i-iv) and an injured one (Fig. 8B, i-iv) at 0, 3, 29, and 50 minutes after injury. To quantify the changes in perfusion over time for each condition and account for the differences in topologies between the two sections of spinal cord, the ROI corresponding to the area of indentation was normalized to a reference area closer to the cannulation site (Fig. 7C). Quantification of the flux heatmap images (Fig. 7D) and linear regression analysis of the BPU averages show a relatively constant level of perfusion through the control section (rate of perfusion

increases at 0.0671/min), compared to the injured section (a rate of 0.6398/minute), which was nearly an order of magnitude higher. These results suggest that the ex vivo model replicates the initial hypoperfusion phase in the spinal cord observed using in vivo ultrasound measurements [53] and that the rate of perfusion increases as a function of time in the injured section.

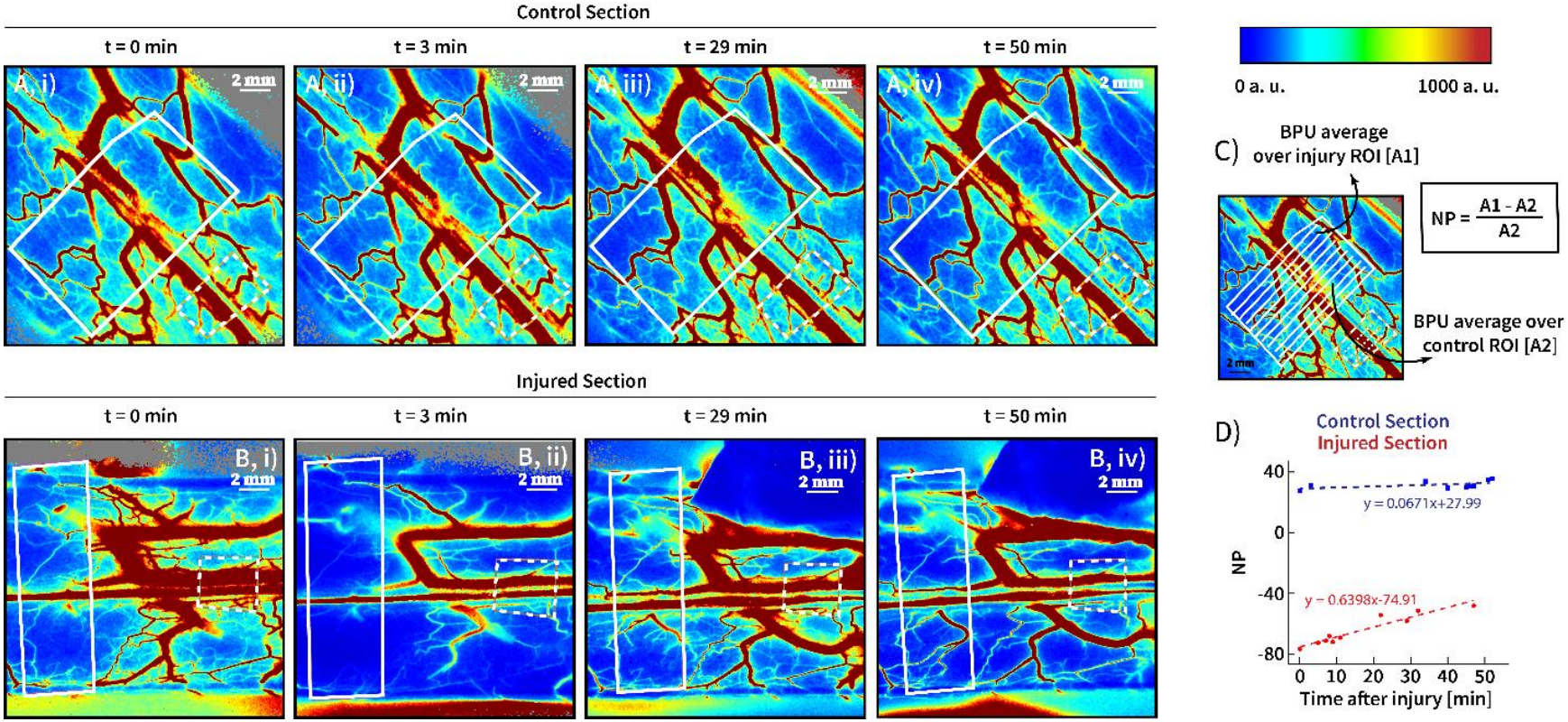

Figure 7. Laser speckle contrast images of bovine spinal cord perfused sections. (A, B) Speckle contrast images of the perfused spinal cord sections for a control (A) and injured (B) section at 0 min (A,i B,i), at 3 minutes (A,ii B,ii), at 29 minutes (A,iii B,iii), at 50 minutes (A,iv B,iv). A schematic of the quantification of normalized flow is provided in (C). Perfusion values over time for both samples with linear regression (D).

Microvascular Integrity

The limitation of LSCI for analyzing perfusion beneath the pial layer necessitated histological evaluation of the integrity of the blood-spinal cord barrier in the parenchyma using Evans Blue perfusion. Figure 8 shows immunohistochemical images of control (Fig. 8A, i-iv) and injured sections (Fig. 8B, i-iv), which was used to quantify Evans blue extravasation and ED-1 expression at 0, 15, 30, and 60 minutes. The comparison of the ratio of Evans blue intensity in the lumen of vasculature and immediate extravascular space showed significant differences between injured and control cords (Fig. 8, A-B). The ratio of Evans blue was significantly higher in the non-injured controls for all four time points, evidence of BSCB breakdown. Moreover, an ANOVA revealed that time was a significant variable, indicating that the barrier function improved over the hour period of whole blood perfusion (Fig. 8C). This increase in barrier function in response to the application of flow is consistent with previous studies indicating that fluid shear stress improves barrier function [48], Comparison of the variance of the ED-1 expression, a marker for microglia activation, in the histological sections also revealed significant differences between control and injured sections, with ED-1 variance significantly higher in the sections exposed to crush injury for all time points (Fig. 8D). The variance was used to account for differences in staining intensity in the sections.

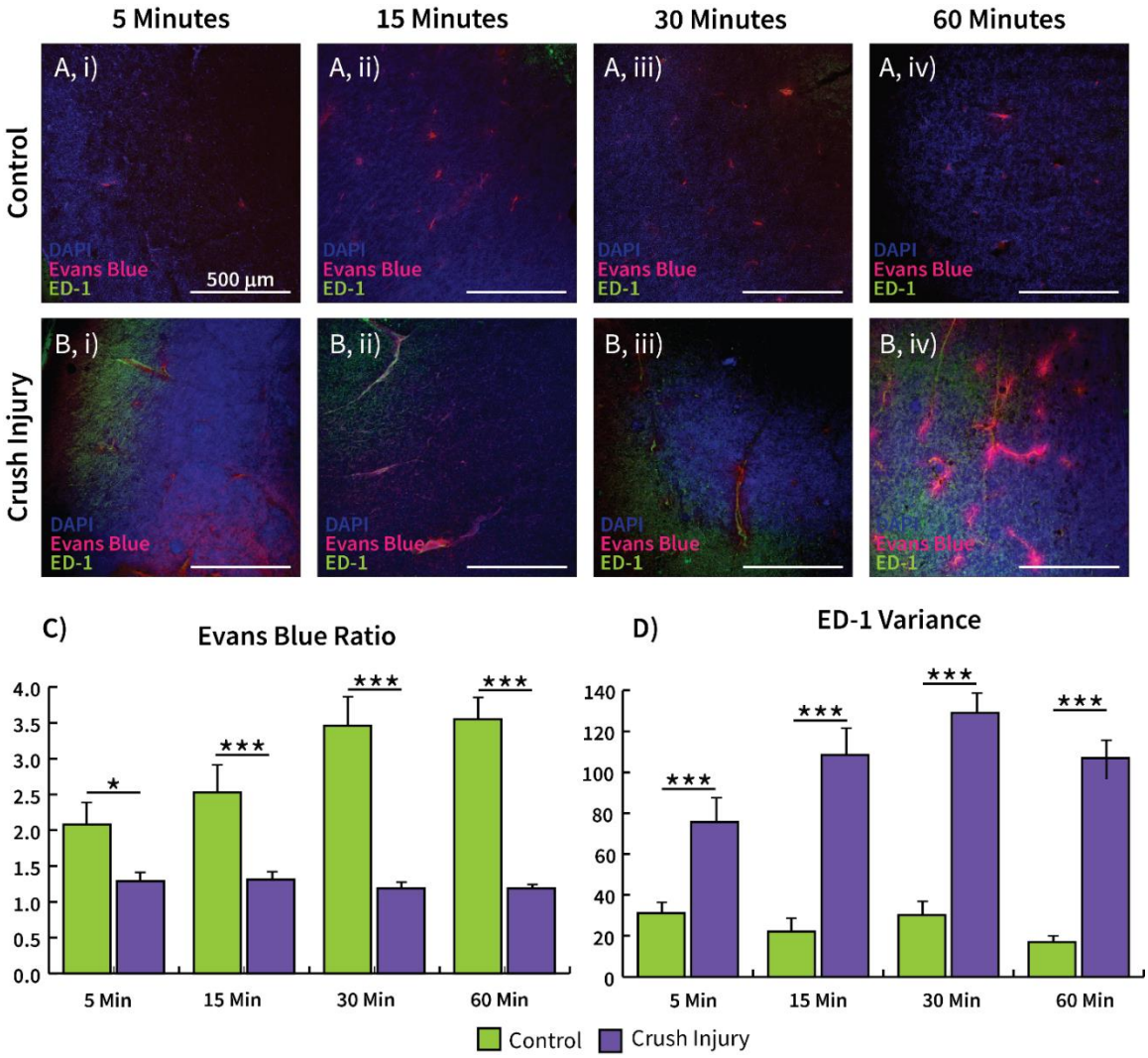

Figure 8. Immunohistochemical images of control (A) and injured (B) section of spinal cord. Images shows DAPI (blue), Evans blue (red), and ED-1 (green) at 5 minutes (A,i B,i), at 15 minutes (A,ii B,ii), at 30 minutes (A,iii B,iii), at 60 minutes (A,iv B,iv). Evans blue ratio results (C) and ED-1 Variance analysis (D).

Vimentin expression also changed immediately after injury in unpermeabilized sections (Fig. 9A,B), as the ratio of vimentin expression in the tissue compared to the area around the blood vessels was higher in the injured section compared to controls at both 5 and 30 minutes (Fig. 9C-D). These results suggest that vimentin expression is an important mediator of the rapid injury response and correlates with breakdown of barrier function.

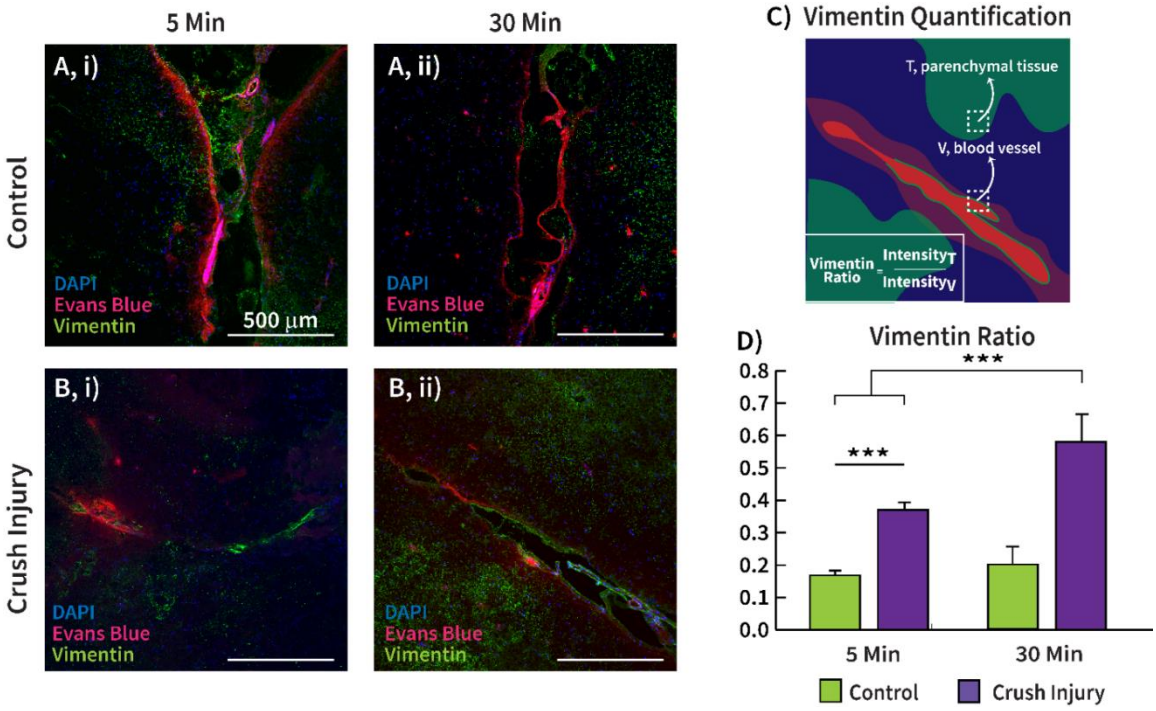

Figure 9. Immunohistochemical staining for DAPI, Evans Blue, and vimentin. Image show control (A) and injured (B) sections of spinal cord tissue at 5 minutes (A,i B,i) and 30 minutes (A,ii B,ii). Intensity ratio quantification of the vimentin signal (C-D) is quantified in part E.

An ELISA was conducted to determine whether plasma levels of vimentin were elevated in the blood perfusing injured cords, given previous studies identifying

extracellular vimentin as a potential immunomodulator [63] and the difference between vimentin staining between control and injured sections. However, the ELISA found no significant difference in the vimentin levels in blood (Fig. 10). Therefore, the source of vimentin and whether it is secreted in its extracellular form remain unclear from these results.

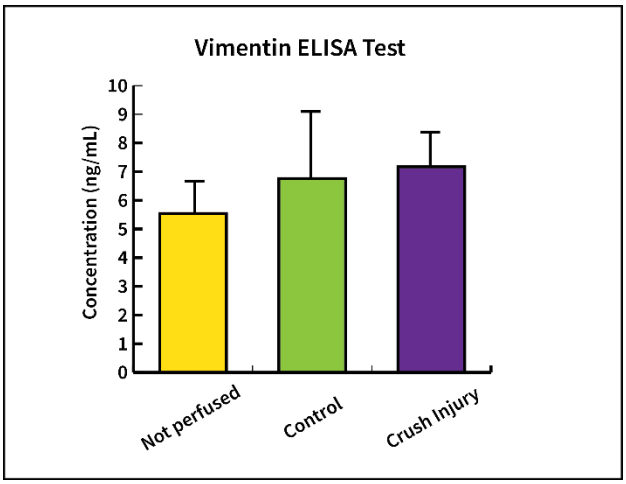

Figure 10. Vimentin ELISA test.

Immunohistochemical staining of vimentin on permeabilized slices produced opposite results compared to images of unpermeabilized slices (Figure 11A,B). In this case, the injured spinal cord sections (Figure 11D) exhibited lower levels of vimentin expression than their control counterparts (Figure 11C), suggesting that vimentin might be expressed on the cell membrane and lost upon membrane permeabilization. However, since the antibody is not specific to extracellular and intracellular vimentin, these results do not clarify the nature of vimentin's extracellular and intracellular forms.

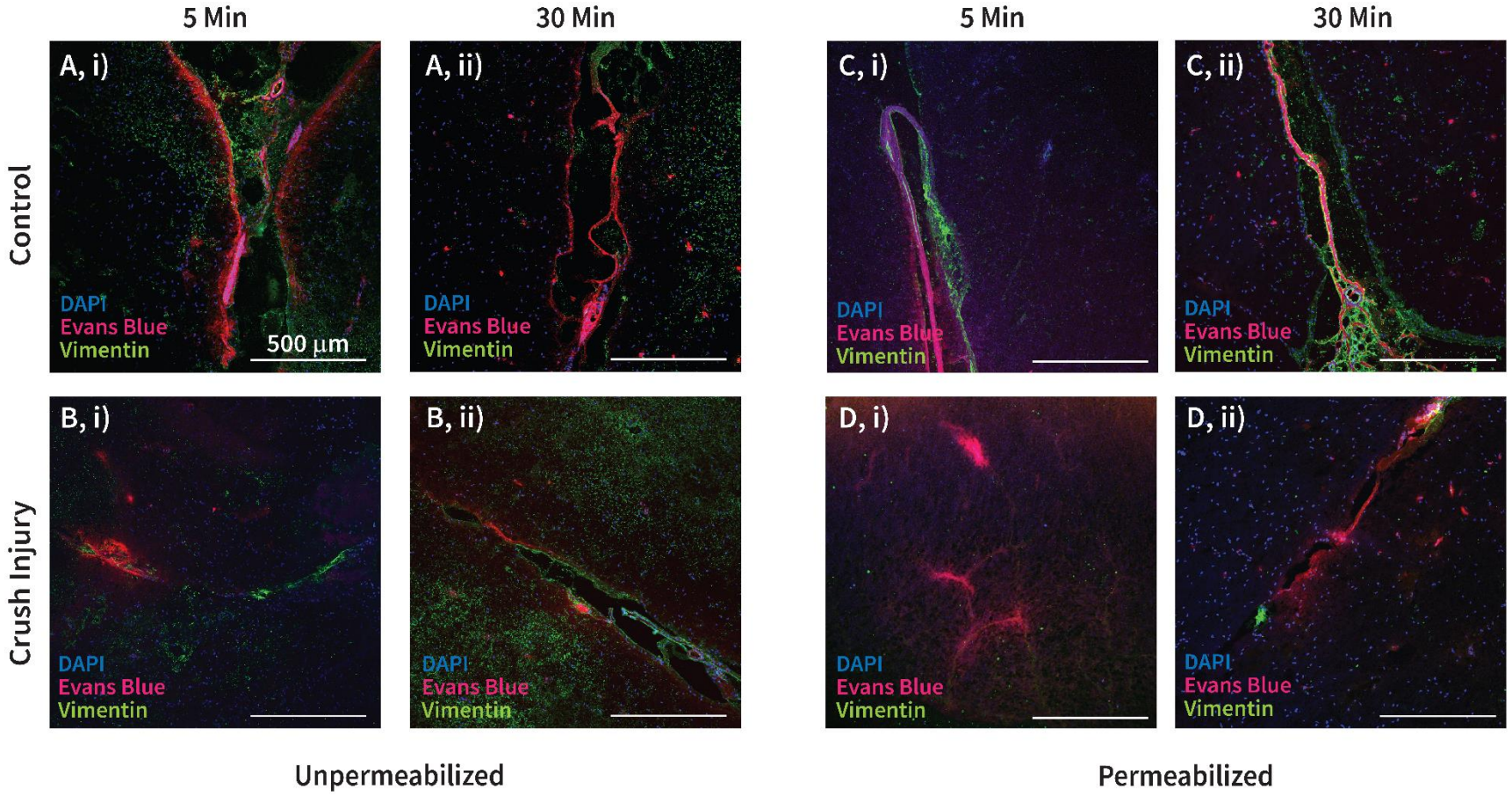

Figure 11. Immunohistochemical staining for DAPI (blue), Evans Blue (magenta), and vimentin (green). Image show control (A,C) and injured (B,D) sections of spinal cord tissue at 5 minutes (A,i B,i, C,i, D,i) and 30 minutes (A,ii B,ii, C,ii, D,ii) for unpermeabilized (A,B) and permeabilized (C,D) slides.

Mechanical Changes Following BSCB Breakdown

The ex vivo model was used to determine whether the changes in blood flow, BSCB integrity, and ED-1 and vimentin expression correlate to altered mechanical properties in the minutes following injury. Initially, the mechanical properties were assessed using tensiometry. Yet, tensiometry testing, which involves indentation on the scale of micrometers, showed no significant difference between the elastic modulus of a perfused section after injury compared to a non-injured control section (Fig. 12A). Given the thickness of the cord and finite element modeling indicating that the stress generated in the tissue by the indenter extends beyond the 6-mm deformation (Fig. 12B), the mechanical indentation used to injure the cord was utilized to measure the elastic modulus with Hertz contact theory (Fig. 4A, B).

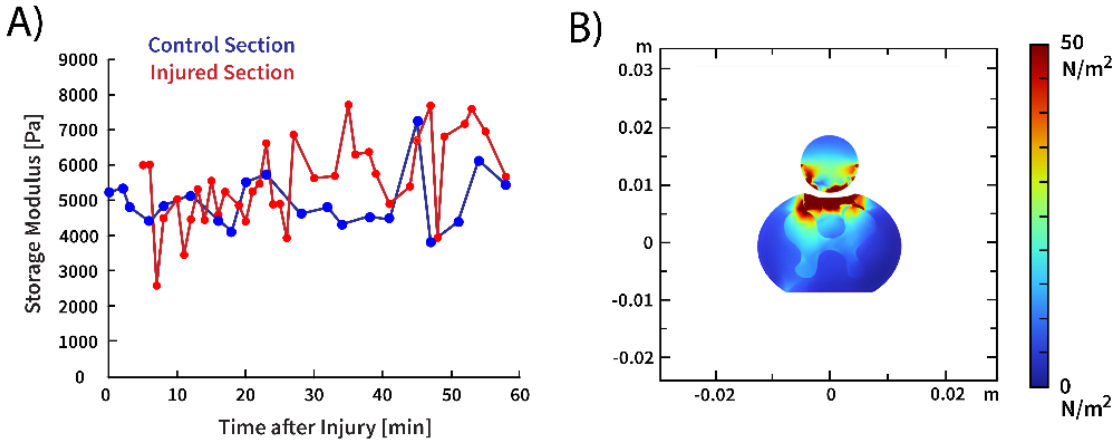

Figure 12. Tensiometry results (A) and COMSOL model for indentation testing (B).

Therefore, the indenter both injures the cord and derives information about its mechanical properties simultaneously. Moreover, the elastic modulus was measured at the

time of injury and then at either 15, 30, or 60 minutes later and the drop in elastic modulus for each cord was calculated. To understand whether temperature could expedite the tissue mechanisms responsible for the loss of mechanical properties, the elastic moduli was measured after 60 minutes in which the sections were either perfused or kept in an aCSF bath at room temperature or at 37˚C. The results suggest that, although perfusion is a key factor in the loss of mechanical properties, temperature does not affect the rapidity at which the elastic moduli start decreasing (Fig. 13A). Additionally, perfusion of the spinal cord with whole blood had significant differences in elastic modulus decrease compared to the sections perfused with reconstituted red blood cells. After 30 minutes of perfusion, the elastic moduli for the sections perfused with whole blood decreased by 23.63% ± 1.31% compared to the 3.4% ± 2.74% of rRBC perfused sections. The elastic moduli decrease significantly increased over time and, at 60 minutes after injury, whole blood perfused sections showed a 41.44% ± 4.91% decrease compared to the 1.05% ± 1.98% decrease of sections perfused with red blood cells only (Fig. 13B). These results suggest that leukocytes and components of the plasma mediate the reduction in tissue stiffness.

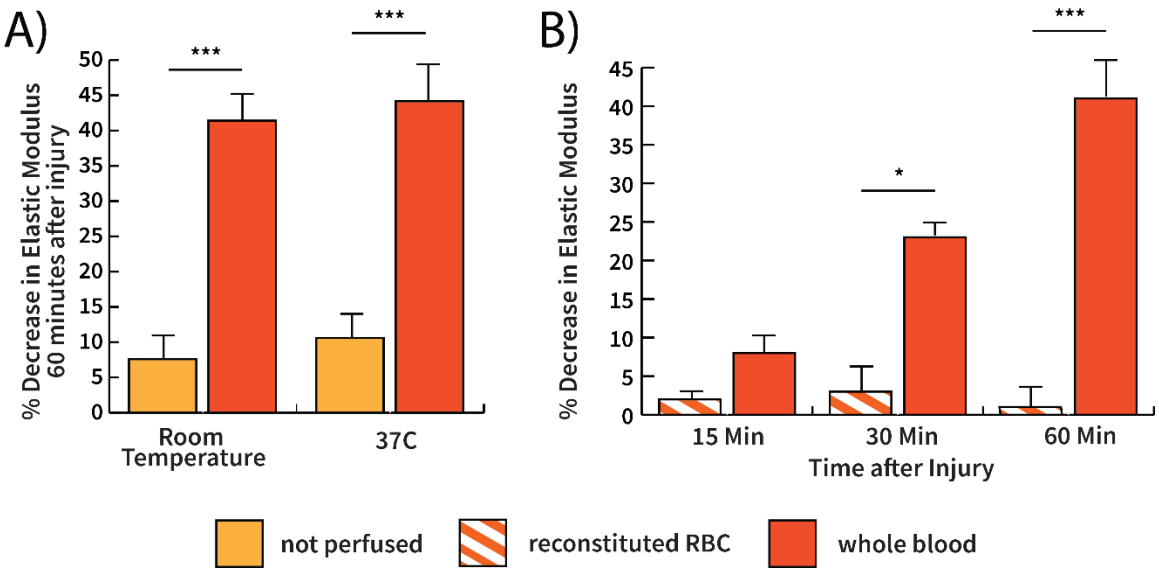

Figure 13. Mechanical testing analysis. (A) Percentage decrease in mechanical properties after 60 minutes from the time of injury in cords non perfused and kept in aCSF baths and cords perfused with whole blood at both room temperature and 37˚C. (B) Percentage decrease in mechanical properties from the time of injury to the second measurement in cords perfused with either whole blood or reconstituted red blood cells.

Chapter 4

Discussion

The perfused ex vivo spinal cord model reveals that mechanical softening begins within minutes of injury and requires whole blood perfusion, highlighting the role of BSCB in the acute injury response. Our results show that spinal cord tissue stiffness is significantly reduced as early as 30 minutes post-SCI, suggesting that the early microglia activation, also observed by other groups, correlates to rapid effects on the mechanical properties of the tissue. Additionally, the significant difference between the elastic moduli of injured sections perfused with whole blood and reconstituted red blood cells over the first hour provides further evidence of the relationship between BSCB breakdown, inflammatory cells infiltration, and changes in tissue stiffness. These findings support previous work stating the importance of leukocyte infiltration in the promotion of ECM remodeling and consequent mechanical degradation [46, 64]. Further experiments are needed to investigate the specific mechanisms by which the extravasation of leukocytes, inflammatory cytokines, and blood components contribute to microglial activation and subsequent reduction of mechanical properties.

Understanding the immune system response to injury and the following ECM remodeling is crucial for developing targeted treatments for SCI. Previous studies have identified microglia as the first responder of spinal cord injury [47, 49], exhibiting activation within the first few minutes after injury [24, 25]. Our immunohistochemical results support these findings by showing presence of activated microglia and Evans blue diffused outside of blood vessels as early as 5 minutes after injury and a significant progression as time increases. Although there is no spatial correlation between the

localization of activated microglia and Evans blue extravasation, their combined presence in the first hour after indentation injury provides evidence that BSCB breakdown is a factor in microglia-mediated ECM remodeling that reduces tissue stiffness.

The contrast between permeabilized and unpermeabilized conditions suggests a variation in vimentin localization within the cells. The permeabilization process, which disrupts extracellular proteins, likely accounts for the observed decrease in vimentin expression, as it leads to the loss of binding receptors. However, the antibody used does not distinctly differentiate between extracellular and intracellular vimentin. Therefore, further experiments are needed to investigate the localization of vimentin following spinal cord injury and to determine its impact on the biological and mechanical responses of the spinal cord. The hypothesis that vimentin is expressed extracellularly after injury supports other findings that show extracellular vimentin triggering an immune response [65] and promoting the recruitment of fibroblasts for wound healing [66, 67]. Additionally, the increase in vimentin expression in the tissue shown in the injured condition supports findings from other groups suggesting that vimentin is released by astrocytes [68] and macrophages [69] after injury as a neurotrophic factor to aid neuron outgrowth [70, 71]. The findings highlight the need for further investigation into vimentin localization and its functional role in spinal cord injury, particularly in relation to its extracellular expression and involvement in immune response and tissue repair.

Overall, the perfused ex vivo indentation model introduces a new platform to investigate short-term consequences of acute injury on the extracellular matrix mechanics of the spinal cord. Our results highlight the importance of including blood perfusion in ex vivo models to better study the relationship between the BSCB disruption and the ECM

mechanical response. Monitoring of superficial and inner vasculature after indentation injury suggests that the ex vivo model mimics in vivo perfusion conditions and is therefore capable of interrogating the short-term consequences of SCI.

Chapter 5

Conclusions

This research highlights the rapid impact of blood-spinal barrier breakdown on the spinal cord tissue mechanics following traumatic injury. Through the perfused ex vivo indentation injury model, we have revealed that the loss of mechanical properties occur within minutes of the primary injury and that white blood cells and plasma proteins are a key factor in the initial loss of tissue stiffness. Understanding the impact of BSCB disruption on the extracellular matrix and mechanical properties of spinal cord tissue in the acute phase of injury is crucial for targeting early cellular mechanisms. This knowledge can help mitigate the inhibitory environment that hinders axonal outgrowth and spinal cord reconnection, improving potential recovery outcomes. Additionally, a more precise characterization of the changes in mechanical properties immediately following the primary injury is essential for developing therapeutic treatments that effectively address these alterations. This understanding can enable the design of interventions that consider these early mechanical changes, potentially improving treatment efficacy.

References

[1] "The 2023 Annual Statistical Report," National Spinal Cord Injury Statistical Center, 2024.

[2] M. Soubeyrand *et al.*, "Preoperative imaging study of the spinal cord vascularization: interest and limits in spine resection for primary tumors," *European journal of radiology,* vol. 77, no. 1, pp. 26-33, 2011.

[3] J. S. Krause, M. Sternberg, S. Lottes, and J. Maides, "Mortality after spinal cord injury: an 11-year prospective study," *Archives of physical medicine and rehabilitation,* vol. 78, no. 8, pp. 815-821, 1997.

[4] M. K. Ganapathy, V. Reddy, and P. Tadi, "Neuroanatomy, spinal cord morphology," 2019.

[5] O. Bican, A. Minagar, and A. A. Pruitt, "The spinal cord: a review of functional neuroanatomy," *Neurologic clinics,* vol. 31, no. 1, pp. 1-18, 2013.

[6] A. Santillan, V. Nacarino, E. Greenberg, H. A. Riina, Y. P. Gobin, and A. Patsalides, "Vascular anatomy of the spinal cord," *Journal of neurointerventional surgery,* vol. 4, no. 1, pp. 67-74, 2012.

[7] S. Cheng, E. C. Clarke, and L. E. Bilston, "Rheological properties of the tissues of the central nervous system: a review," *Medical engineering & physics,* vol. 30, no. 10, pp. 1318-1337, 2008.

[8] S. Chatelin, A. Constantinesco, and R. Willinger, "Fifty years of brain tissue mechanical testing: from in vitro to in vivo investigations," *Biorheology,* vol. 47, no. 5-6, pp. 255-276, 2010.

[9] Y. K. Mariappan, K. J. Glaser, and R. L. Ehman, "Magnetic resonance elastography: a review," *Clinical anatomy,* vol. 23, no. 5, pp. 497-511, 2010.

[10] A. Di Ieva *et al.*, "Magnetic resonance elastography: a general overview of its current and future applications in brain imaging," *Neurosurgical review,* vol. 33, pp. 137-145, 2010.

[11] K. Ichihara, T. Taguchi, Y. Shimada, I. Sakuramoto, S. Kawano, and S. Kawai, "Gray matter of the bovine cervical spinal cord is mechanically more rigid and fragile than the white matter," *Journal of neurotrauma,* vol. 18, no. 3, pp. 361-367, 2001.

[12] L. E. Bilston and L. E. Thibault, "The mechanical properties of the human cervical spinal cord in vitro," *Annals of biomedical engineering,* vol. 24, pp. 67-74, 1995.

[13] D. E. Koser, E. Moeendarbary, J. Hanne, S. Kuerten, and K. Franze, "CNS cell distribution and axon orientation determine local spinal cord mechanical properties," *Biophysical journal,* vol. 108, no. 9, pp. 2137-2147, 2015.

[14] K. A. Tran *et al.*, "Matching mechanical heterogeneity of the native spinal cord augments axon infiltration in 3D-printed scaffolds," *Biomaterials,* vol. 295, p. 122061, 2023.

[15] C. S. Ahuja *et al.*, "Traumatic spinal cord injury," *Nature reviews Disease primers,* vol. 3, no. 1, pp. 1-21, 2017.

[16] R. J. Dumont *et al.*, "Acute spinal cord injury, part I: pathophysiologic mechanisms," *Clinical neuropharmacology,* vol. 24, no. 5, pp. 254-264, 2001.

[17] L. H. Sekhon and M. G. Fehlings, "Epidemiology, demographics, and pathophysiology of acute spinal cord injury," *Spine,* vol. 26, no. 24S, pp. S2-S12, 2001.

[18] J. Bennett and P. Emmady, "Spinal cord injuries," 2020.

[19] A. Min-Te Choo, J. Liu, Z. Liu, M. Dvorak, W. Tetzlaff, and T. R. Oxland, "Modeling spinal cord contusion, dislocation, and distraction: characterization of vertebral clamps, injury severities, and node of Ranvier deformations," *Journal of neuroscience methods,* vol. 181, no. 1, pp. 6-17, 2009.

[20] A. Alizadeh, S. M. Dyck, and S. Karimi-Abdolrezaee, "Traumatic spinal cord injury: an overview of pathophysiology, models and acute injury mechanisms," *Frontiers in neurology,* vol. 10, p. 441408, 2019.

[21] X. Z. Liu *et al.*, "Neuronal and glial apoptosis after traumatic spinal cord injury," *Journal of Neuroscience,* vol. 17, no. 14, pp. 5395-5406, 1997.

[22] M. C. LaPlaca, C. Simon, G. R. Prado, and D. Cullen, "CNS injury biomechanics and experimental models," *Progress in brain research,* vol. 161, pp. 13-26, 2007.

[23] I. Pineau and S. Lacroix, "Proinflammatory cytokine synthesis in the injured mouse spinal cord: multiphasic expression pattern and identification of the cell types involved," *Journal of Comparative Neurology,* vol. 500, no. 2, pp. 267-285, 2007.

[24] A. Nimmerjahn, F. Kirchhoff, and F. Helmchen, "Resting microglial cells are highly dynamic surveillants of brain parenchyma in vivo," *Science,* vol. 308, no. 5726, pp. 1314-1318, 2005.

[25] D. Davalos *et al.*, "ATP mediates rapid microglial response to local brain injury in vivo," *Nature neuroscience,* vol. 8, no. 6, pp. 752-758, 2005.

[26] Y. Wang, H. Wang, Y. Tao, S. Zhang, J. Wang, and X. Feng, "Necroptosis inhibitor necrostatin-1 promotes cell protection and physiological function in traumatic spinal cord injury," *Neuroscience,* vol. 266, pp. 91-101, 2014.

[27] M. D. Norenberg, J. Smith, and A. Marcillo, "The pathology of human spinal cord injury: defining the problems," *Journal of neurotrauma,* vol. 21, no. 4, pp. 429-440, 2004.

[28] C. S. Ahuja, A. R. Martin, and M. Fehlings, "Recent advances in managing a spinal cord injury secondary to trauma," *F1000Research,* vol. 5, 2016.

[29] R. J. McKeon, R. C. Schreiber, J. S. Rudge, and J. Silver, "Reduction of neurite outgrowth in a model of glial scarring following CNS injury is correlated with the expression of inhibitory molecules on reactive astrocytes," *Journal of Neuroscience,* vol. 11, no. 11, pp. 3398-3411, 1991.

[30] M. A. Anderson *et al.*, "Astrocyte scar formation aids central nervous system axon regeneration," *Nature,* vol. 532, no. 7598, pp. 195-200, 2016.

[31] S. Karimi-Abdolrezaee and R. Billakanti, "Reactive astrogliosis after spinal cord injury—beneficial and detrimental effects," *Molecular neurobiology,* vol. 46, pp. 251-264, 2012.

[32] E. Moeendarbary *et al.*, "The soft mechanical signature of glial scars in the central nervous system," *Nature communications,* vol. 8, no. 1, p. 14787, 2017.

[33] C. Jin *et al.*, "Dynamic changes in mechanical properties of the adult rat spinal cord after injury," *Acta biomaterialia,* vol. 155, pp. 436-448, 2023.

[34] J. Silver and J. H. Miller, "Regeneration beyond the glial scar," *Nature reviews neuroscience,* vol. 5, no. 2, pp. 146-156, 2004.

[35] J. Zhu *et al.*, "Mechanical matching nanofibrous vascular scaffold with effective anticoagulation for vascular tissue engineering," *Composites Part B: Engineering,* vol. 186, p. 107788, 2020.

[36] J. Wieding, A. Wolf, and R. Bader, "Numerical optimization of open-porous bone scaffold structures to match the elastic properties of human cortical bone," *Journal of the mechanical behavior of biomedical materials,* vol. 37, pp. 56-68, 2014.

[37] L. Hidalgo-Bastida *et al.*, "Cell adhesion and mechanical properties of a flexible scaffold for cardiac tissue engineering," *Acta biomaterialia,* vol. 3, no. 4, pp. 457-462, 2007.

[38] I. R. Minev *et al.*, "Electronic dura mater for long-term multimodal neural interfaces," *Science,* vol. 347, no. 6218, pp. 159-163, 2015.

[39] P. Moshayedi *et al.*, "The relationship between glial cell mechanosensitivity and foreign body reactions in the central nervous system," *Biomaterials,* vol. 35, no. 13, pp. 3919-3925, 2014.

[40] A. Bakshi, O. Fisher, T. Dagci, B. T. Himes, I. Fischer, and A. Lowman, "Mechanically engineered hydrogel scaffolds for axonal growth and angiogenesis after transplantation in spinal cord injury," *Journal of Neurosurgery: Spine,* vol. 1, no. 3, pp. 322-329, 2004.

[41] J.-S. Cho *et al.*, "Transplantation of mesenchymal stem cells enhances axonal outgrowth and cell survival in an organotypic spinal cord slice culture," *Neuroscience letters,* vol. 454, no. 1, pp. 43-48, 2009.

[42] F. Doussau, J.-L. Dupont, D. Neel, A. Schneider, B. Poulain, and J. L. Bossu, "Organotypic cultures of cerebellar slices as a model to investigate demyelinating disorders," *Expert Opinion on Drug Discovery,* vol. 12, no. 10, pp. 1011-1022, 2017.

[43] T. Fernandez-Zafra, S. Codeluppi, and P. Uhlén, "An ex vivo spinal cord injury model to study ependymal cells in adult mouse tissue," *Experimental Cell Research,* vol. 357, no. 2, pp. 236-242, 2017.

[44] S. Pandamooz, M. Nabiuni, J. Miyan, A. Ahmadiani, and L. Dargahi, "Organotypic spinal cord culture: a proper platform for the functional screening," *Molecular neurobiology,* vol. 53, pp. 4659-4674, 2016.

[45] M.-S. Guzman-Lenis, X. Navarro, and C. Casas, "Drug screening of neuroprotective agents on an organotypic-based model of spinal cord excitotoxic damage," *Restorative neurology and neuroscience,* vol. 27, no. 4, pp. 335-349, 2009.

[46] A. M. Choo, J. Liu, C. K. Lam, M. Dvorak, W. Tetzlaff, and T. R. Oxland, "Contusion, dislocation, and distraction: primary hemorrhage and membrane permeability in distinct mechanisms of spinal cord injury," *Journal of Neurosurgery: Spine,* vol. 6, no. 3, pp. 255-266, 2007.

[47] D. J. Donnelly and P. G. Popovich, "Inflammation and its role in neuroprotection, axonal regeneration and functional recovery after spinal cord injury," *Experimental neurology,* vol. 209, no. 2, pp. 378-388, 2008.

[48] P. P. Partyka *et al.*, "Mechanical stress regulates transport in a compliant 3D model of the blood-brain barrier," *Biomaterials,* vol. 115, pp. 30-39, 2017.

[49] P. G. Popovich and W. F. Hickey, "Bone marrow chimeric rats reveal the unique distribution of resident and recruited macrophages in the contused rat spinal cord," *Journal of Neuropathology & Experimental Neurology,* vol. 60, no. 7, pp. 676-685, 2001.

[50] Y. Xu *et al.*, "Quantifying blood-brain-barrier leakage using a combination of evans blue and high molecular weight FITC-Dextran," *Journal of neuroscience methods,* vol. 325, p. 108349, 2019.

[51] J. Senarathna, A. Rege, N. Li, and N. V. Thakor, "Laser speckle contrast imaging: theory, instrumentation and applications," *IEEE reviews in biomedical engineering,* vol. 6, pp. 99-110, 2013.

[52] F. Lesage, N. Brieu, S. Dubeau, and E. Beaumont, "Optical imaging of vascular and metabolic responses in the lumbar spinal cord after T10 transection in rats," *Neuroscience letters,* vol. 454, no. 1, pp. 105-109, 2009.

[53] Z. Z. Khaing *et al.*, "Contrast-enhanced ultrasound for assessment of local hemodynamic changes following a rodent contusion spinal cord injury," *Military Medicine,* vol. 185, no. Supplement_1, pp. 470-475, 2020.

[54] Z. Z. Khaing, L. N. Cates, J. E. Hyde, R. Hammond, M. Bruce, and C. P. Hofstetter, "Transcutaneous contrast-enhanced ultrasound imaging of the posttraumatic spinal cord," *Spinal cord,* vol. 58, no. 6, pp. 695-704, 2020.

[55] M. Soubeyrand, A. Badner, R. Vawda, Y. S. Chung, and M. G. Fehlings, "Very high resolution ultrasound imaging for real-time quantitative visualization of vascular disruption after spinal cord injury," *Journal of Neurotrauma,* vol. 31, no. 21, pp. 1767-1775, 2014.

[56] Z. Z. Khaing *et al.*, "Contrast-enhanced ultrasound to visualize hemodynamic changes after rodent spinal cord injury," *Journal of Neurosurgery: Spine,* vol. 29, no. 3, pp. 306-313, 2018.

[57] E. Hernandez-Andrade *et al.*, "Evaluation of cervical stiffness during pregnancy using semiquantitative ultrasound elastography," *Ultrasound in Obstetrics & Gynecology,* vol. 41, no. 2, pp. 152-161, 2013.

[58] T. Inami and Y. Kawakami, "Assessment of individual muscle hardness and stiffness using ultrasound elastography," *The Journal of Physical Fitness and Sports Medicine,* vol. 5, no. 4, pp. 313-317, 2016.

[59] J. E. Brandenburg *et al.*, "Ultrasound elastography: the new frontier in direct measurement of muscle stiffness," *Archives of physical medicine and rehabilitation,* vol. 95, no. 11, pp. 2207-2219, 2014.

[60] H. M. DeJong, S. Abbott, M. Zelesco, B. F. Kennedy, M. R. Ziman, and F. M. Wood, "The validity and reliability of using ultrasound elastography to measure cutaneous stiffness, a systematic review," *International journal of burns and trauma,* vol. 7, no. 7, p. 124, 2017.

[61] J. Prager *et al.*, "Stiffness-matched biomaterial implants for cell delivery: clinical, intraoperative ultrasound elastography provides a 'target'stiffness for hydrogel synthesis in spinal cord injury," *Journal of tissue engineering,* vol. 11, p. 2041731420934806, 2020.

[62] S. Tang *et al.*, "Assessment of spinal cord injury using ultrasound elastography in a rabbit model in vivo," *Scientific Reports,* vol. 13, no. 1, p. 15323, 2023.

[63] Ł. Suprewicz *et al.*, "Extracellular vimentin as a modulator of the immune response and an important player during infectious diseases," *Immunology and Cell Biology,* 2024.

[64] D. McCreedy *et al.*, "Early targeting of L-selectin on leukocytes promotes recovery after spinal cord injury, implicating novel mechanisms of pathogenesis," *eneuro,* vol. 5, no. 4, 2018.

[65] I. Ramos, K. Stamatakis, C. L. Oeste, and D. Pérez-Sala, "Vimentin as a multifaceted player and potential therapeutic target in viral infections," *International journal of molecular sciences,* vol. 21, no. 13, p. 4675, 2020.

[66] M. Shigyo, T. Kuboyama, Y. Sawai, M. Tada-Umezaki, and C. Tohda, "Extracellular vimentin interacts with insulin-like growth factor 1 receptor to promote axonal growth," *Scientific reports,* vol. 5, no. 1, p. 12055, 2015.

[67] J. Walker, B. Bleaken, A. Romisher, A. Alnwibit, and A. Menko, "In wound repair vimentin mediates the transition of mesenchymal leader cells to a myofibroblast phenotype," *Molecular biology of the cell,* vol. 29, no. 13, pp. 1555-1570, 2018.

[68] O. Cordero-Llana *et al.*, "Clusterin secreted by astrocytes enhances neuronal differentiation from human neural precursor cells," *Cell Death & Differentiation,* vol. 18, no. 5, pp. 907-913, 2011.

[69] N. Mor-Vaknin, A. Punturieri, K. Sitwala, and D. M. Markovitz, "Vimentin is secreted by activated macrophages," *Nature cell biology,* vol. 5, no. 1, pp. 59-63, 2003.

[70] M. Shigyo and C. Tohda, "Extracellular vimentin is a novel axonal growth facilitator for functional recovery in spinal cord-injured mice," *Scientific Reports,* vol. 6, no. 1, p. 28293, 2016.

[71] K. Teshigawara *et al.*, "A novel compound, denosomin, ameliorates spinal cord injury via axonal growth associated with astrocyte-secreted vimentin," *British journal of pharmacology,* vol. 168, no. 4, pp. 903-919, 2013.